

Spatiotemporal Analysis of NO Production upon NMDA and Tetanic Stimulation of the Hippocampus

Norio Takata, Tokiko Harada, John A. Rose, and Suguru Kawato*

ABSTRACT: Nitric oxide (NO) is a gaseous neuromessenger. Although increasing evidence reveals significant physiological effects of NO in the hippocampal synaptic plasticity, the spatial distribution of NO production has remained largely uncharacterized due to the poor development of techniques for real-time NO imaging. In this work, using a NO-reactive fluorescent dye, diaminorhodamine-4M (DAR-4M), time-dependent heterogeneous NO production is demonstrated in hippocampal slices upon N-methyl-D-aspartate (NMDA) stimulation or tetanic stimulation. NMDA-induced DAR fluorescence increase in the CA1 was found to be twice that in the CA3 and the dentate gyrus (DG). Intracellular Ca^{2+} concentration was also investigated. NMDA induced similar Ca^{2+} responses both in the CA1 and DG, which were approx. 13% greater than that in the CA3. Subsequently, spatial distribution of NO production in the CA1 upon a tetanic stimulation of Schaffer collateral was investigated, because there are contradictory reports on the effect of NO on long-term potentiation (LTP), and that NO is known to exert various physiological effects depending on its concentration. In the stratum radiatum (sr), DAR fluorescence increase upon tetanus was largest at the vicinity of a stimulating electrode and decreased as a function of increasing distance from the stimulating electrode, suggesting the possibility that the effect of NO in LTP is dependent on the distance between stimulating and recording electrodes. The tetanus-induced Ca^{2+} response observed in the sr showed the same but weak distant dependence from the stimulating electrode. Taken together, the observed heterogeneity in the distribution of NO production is suggestive of region-specific effects of NO in the hippocampus. © 2005 Wiley-Liss, Inc.

KEY WORDS: nitric oxide; DAR; imaging; tetanus; slice

INTRODUCTION

Nitric oxide (NO), which is synthesized by NO synthase (NOS) (Andrew and Mayer, 1999), is known to act as an intercellular and intracellular

Department of Biophysics and Life Sciences, Core Research for Evolutional Science and Technology Project of Japan Science and Technology Agency, Graduate School of Arts and Sciences, University of Tokyo, Meguro, Tokyo, Japan

Abbreviations used: ACSF, artificial cerebrospinal fluid; DAF-2, diaminofluorescein-2; DAF-FM, diaminofluorescein-FM; DAR-4M, diaminorhodamine-4M; DG, dentate gyrus; eNOS, endothelial NOS; EPSP, excitatory postsynaptic potential; gl, granular layer; LTP, long-term potentiation; ml, molecular layer; NMDA, N-methyl-D-aspartate; nNOS, neuronal NO synthase; NO, nitric oxide; pcl, pyramidal cell layer; pl, polymorphic layer; PTP, posttetanic potentiation; so, stratum oriens; sr, stratum radiatum.

Grant sponsor: Ministry of Education, Science and Technology, Japan; Grant sponsor: Narishige Neuroscience Research Foundation; Grant sponsor: Japan Society for the Promotion of Science.

*Correspondence to: Suguru Kawato, Department of Biophysics and Life Sciences, Graduate School of Arts and Sciences, University of Tokyo at Komaba, 3-8-1 Komaba, Meguro, Tokyo 153-8902, Japan.

E-mail: kawato@phys.c.u-tokyo.ac.jp

Accepted for publication 22 November 2004

DOI 10.1002/hipo.20064

Published online 24 January 2005 in Wiley InterScience (www.interscience.wiley.com).

messenger (Yun et al., 1996). The neuronal form of NOS (nNOS) is present in pyramidal neurons in the CA1 and CA3, and in granular neurons in the dentate gyrus (DG) (Endoh et al., 1994; Iwase et al., 1998; Takata et al., 2002). Because nNOS is a Ca^{2+} /calmodulin-dependent enzyme, linked to NMDA receptors by a scaffold protein, PSD-95 (Christopherson et al., 1999), its synthetic activity is likely to be regulated by the influx of Ca^{2+} through N-methyl-D-aspartate (NMDA) receptors.

NO has been reported to be essentially involved in long-term potentiation (LTP) in the hippocampus (Hawkins et al., 1998; Prast and Philippu, 2001). In the CA1, LTP induction in the stratum radiatum was reportedly suppressed by a NOS inhibitor, although that in stratum oriens was unaffected (Haley et al., 1996). In the CA3, a NOS inhibitor was reported to suppress LTP in the distal apical dendrites, which receive associational–commissural inputs, but not to inhibit LTP in the proximal apical dendrites, which receive mossy fiber inputs (Nicolarakis et al., 1994). In the DG, LTP at the synapses of the perforant pathway was prevented by a NOS inhibitor (Mizutani et al., 1993; Wu et al., 1997). In addition, the physiological effects of NO are known to be concentration-dependent. High NO concentrations stimulate the release of neurotransmitters such as glutamate or GABA, while low concentrations inhibit this release (Prast and Philippu, 2001). These results imply that both the level of NO production and the role played by NO may differ from region to region in the hippocampus. Taken together, these results suggest the importance of addressing how much, and where NO is produced. As the induction of LTP at nearly all hippocampal synapses (with the exception of those in mossy fiber pathways) depends on the influx of Ca^{2+} through NMDA receptors (Nicoll and Malenka, 1995), and because this influx also activates nNOS (Bredt and Snyder, 1990; Takata et al., 2002), the observation of differences in the spatiotemporal pattern of NMDA-induced NO production in different hippocampal regions should be suggestive of different roles for NO in LTP among these regions.

In the present study, we employed a newly synthesized NO-reactive fluorescent dye, DAR-4M (Kojima et al., 2001), in order to compare the NO production upon NMDA stimulation in the CA1, CA3, and DG. In addition, we analyzed the NO production upon tetanic stimulation of the CA1, the area in which the most intensive research on the relationship between LTP and NO has been focused. In each case, the accompanying Ca^{2+} response was

measured to facilitate explanation of differences in the DAR fluorescence increase observed in the various hippocampal regions.

MATERIALS AND METHODS

Chemicals

The acetoxymethyl derivative of DAR-4M (DAR-4M/AM) (Kojima et al., 2001) was purchased from Daiichi Pure Chemicals (Tokyo, Japan), fura-2 AM from Dojindo (Kumamoto, Japan), MK-801 from Sigma (St. Louis, MO), NMDA from RBI (Natick, MA), and L-NMMA from Wako Pure Chemical Industries (Osaka, Japan). All other chemicals were of the highest purity commercially available.

Preparation of Hippocampal Slices

Male Wistar rats aged 8 weeks (purchased from Saitama Experimental Animal Supply, Saitama, Japan) were deeply anesthetized with ethyl ether and decapitated. The brains were quickly removed and placed in O₂ equilibrated artificial cerebrospinal fluid (ACSF) at 2–4°C. The hippocampus was dissected and 400 μ m transverse slices were prepared with a vibratome (DSK ZERO 1, Dosaka, Osaka, Japan) at 0°C. Slices were then incubated in ACSF at room temperature for 1 h. ACSF consisted of (in mM): 127 NaCl, 1.6 KCl, 1.24 KH₂PO₄, 1.3 MgSO₄, 2.4 CaCl₂, 26 NaHCO₃, 10 glucose and was equilibrated with 95% O₂/5% CO₂. All experiments using animals were conducted in accordance with the institutional guidelines.

Slice Loading With Fluorescence Indicators

Hippocampal slices were incubated for 60 min in a plastic tube containing 6 ml of 10 μ M DAR-4M/AM or fura-2 AM (taken from a stock solution in dimethylsulfoxide [DMSO]) filled with 95% O₂ and 5% CO₂ at room temperature. After dye loading, slices were post-incubated in ACSF for at least 30 min. After incorporation into cells, DAR-4M/AM and fura-2 AM were hydrolyzed by nonspecific intracellular esterases to yield membrane impermeant DAR-4M and fura-2, respectively.

Fluorescence Imaging and Analysis

After post-incubation, slices were transferred to a fluorescence recording chamber perfused with 95% O₂/5% CO₂ equilibrated ACSF. The perfusion rate was 1.5 ml/min, and the perfusates were maintained at 30°C throughout each experiment. For measurements of either NMDA-induced NO production or Ca²⁺ response, fluorescence imaging was conducted using a fluorescence microscope consisting of an inverted microscope (TMD 300, Nikon, Tokyo, Japan) and an intensified CCD camera (C2400-77, Hamamatsu Photonics, Hamamatsu, Japan). A 20 \times , 0.75 numerical aperture was used for the fluorescence objective. A cooled CCD camera (ORCA-ER, Hamamatsu Photonics, Hamamatsu, Japan) was employed for measurement of both the NO production, and the Ca²⁺ response induced upon tetanic stimulation.

The microscope chamber maintained an air temperature of 30°C around the sample, using a warm air supply.

During measurements of NO production, DAR-4M was excited at 520–540 nm. The fluorescence above 560 nm was measured using an IF excitation filter, a DM550 dichroic mirror, and a BA560 emission filter (Nikon, Tokyo, Japan). It should be noted that (1) although NO-bound DAR-4M (DAR-4M T) exhibits a bright fluorescence response, NO-free DAR-4M exhibits almost no fluorescence; (2) the reaction of NO and DAR is irreversible (i.e., so that once fluorescence intensity of DAR is increased via reaction with NO, the fluorescence intensity remains).

During measurements of the NMDA-induced NO production, fluorescence images at 520–540 nm were acquired at a rate of 0.2 Hz with an exposure time of 1 s. The time resolution of the measurements was thus 5 s. Images were analyzed using ARGUS-50 software (Hamamatsu Photonics, Hamamatsu, Japan). Acquired images were stored on hard disk, using a 512 \times 482-pixel array, with resolution at an 8-bit depth. The time-dependent fluorescence intensity, $f(t)$ was calculated for each square region (100 \times 100 pixels; Fig. 1A). The NO production at each time, t was estimated by the subtraction of consecutive fluorescence intensities, i.e., $\Delta f(t) = f(t+5 \text{ s}) - f(t \text{ s})$.

For measurements of tetanic stimulation-induced NO production, fluorescence images at 520–540 nm were acquired at a rate of 0.5 Hz with an exposure time of 1 s. The time resolution of the measurements was thus 2 s. Images were analyzed using AQUA COSMOS software (Hamamatsu Photonics, Hamamatsu, Japan). Acquired images were stored on hard disk, using a 128 \times 128-pixel resolution at 16-bit depth. The time-dependent fluorescence intensity, $f(t)$ was calculated for a square region (20 \times 20 or 20 \times 60

FIGURE 1. NMDA-induced DAR fluorescence increase in the CA1, CA3, and DG. **A:** Region used for imaging of NMDA-induced NO. **Top left:** Illustration of a hippocampal slice. Red square indicates the region for imaging; **(top right)** Brightfield image of the CA1 of a DAR-4M-loaded hippocampal slice. Squares 1–4, 5–8, and 9–12 are placed at the so, pcl, and sr, respectively. The slightly bright line running from left to right is the pcl. **Bottom right:** Brightfield image of the CA3. Squares 1–4, 5–8, and 9–12 are placed at the so, pcl, and sr, respectively. The slightly bright line running from top to bottom is the pcl; **(bottom left)** Brightfield image of the dentate gyrus (DG). Squares 1–4, 5–8, and 9–12 are placed at the ml, gl, and pl, respectively. The slightly bright line running from top right to bottom left is the gl. **B:** Time course of DAR-4M fluorescence intensity, averaged over squares 1–12 in Figure 1A for the CA1 upon NMDA stimulation. **C:** Time course of DAR fluorescence increase [$\Delta f(t)$] obtained by subtracting consecutive pairs of DAR-4M fluorescence intensity [$f(t)$] in the CA1. Closed bar above the graph indicates the period of NMDA perfusion. Data depict averages (\pm SD) from six slices. **D:** Time course of DAR fluorescence increase in the presence of a NOS inhibitor. Hippocampal slices were perfused with ACSF containing 300 μ M L-NMMA from 20 min before NMDA stimulation to the end of the measurement, as indicated by a hatched line above the graph. **E:** Comparison of the gross DAR fluorescence increase induced by the stimulation in the presence or absence of a NOS inhibitor. The gross increase was obtained by summing the DAR fluorescence increase [$\Delta f(t)$] from the beginning of NMDA stimulation to 1.5 min after the stimulation. * $P < 0.05$. Data are averages (\pm SD) from six slices. Scale bar = 100 μ m in A. [Color figure can be viewed in the online issue, which is available at www.interscience.wiley.com.]

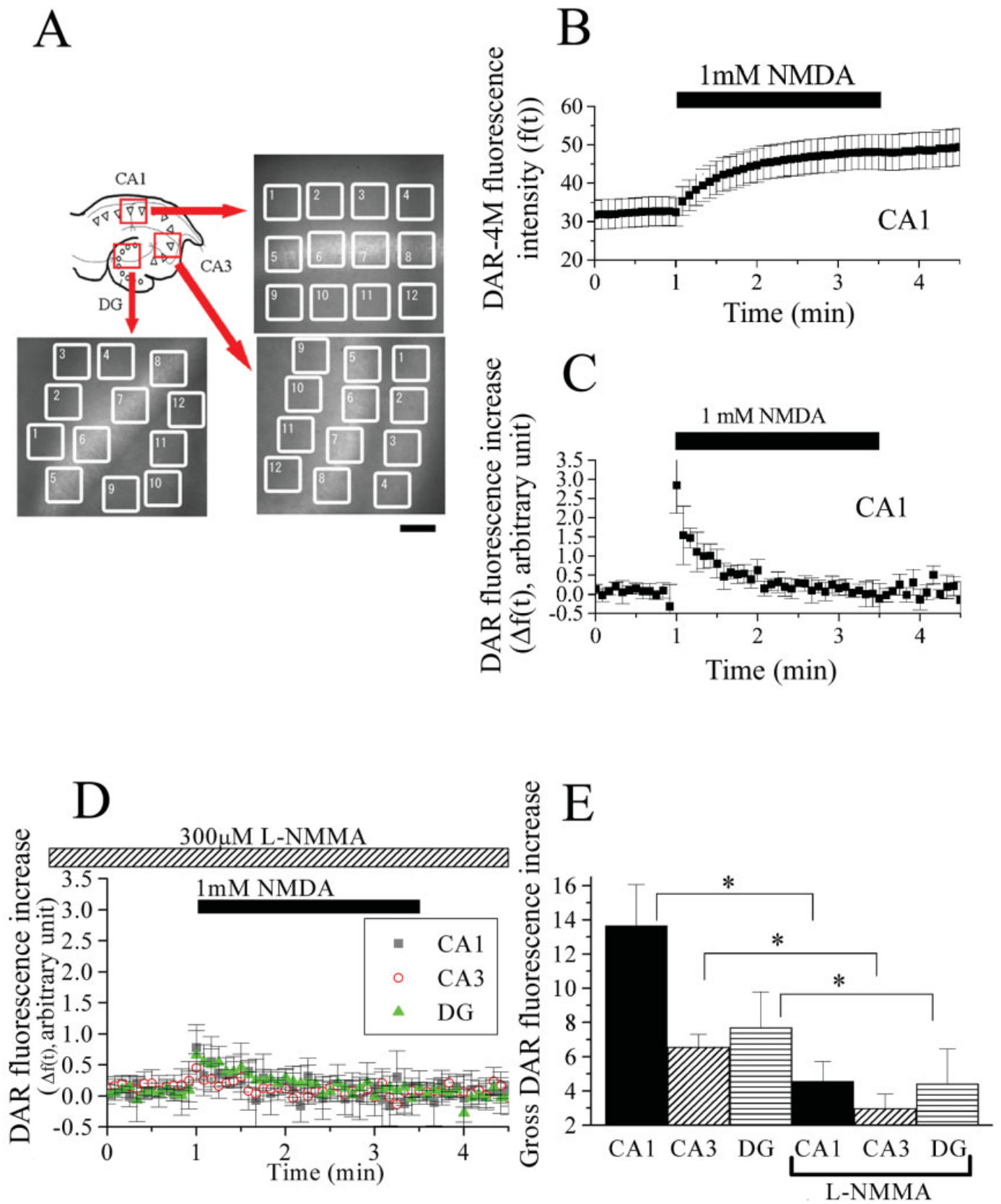


FIGURE 1

pixels; see Fig. 4A). Transient NO production at each time, t was estimated by subtraction of consecutive fluorescence intensities, i.e., $\Delta f(t) = f(t+2 \text{ s}) - f(t \text{ s})$. To improve the signal-to-noise ratio, the time course of the DAR fluorescence intensity was fitted via linear regression (before tetanic stimulation) and sixth-order polynomial regression (after stimulation). The coefficient of determination (R-Square) was larger than 0.96. The curve-fitting was performed with the programs, Excel 2000 (Microsoft, Redmond, WA) and Origin 5.0J (OriginLab, Northampton, MA). For tetanic stimulation, a single pulsed stimulus (20 V) (SanMartin et al., 1999) at 100 Hz was delivered for 1 s (stimulus duration, 100 μ s) with a monopolar tungsten-stimulating electrode placed along the Schaffer collateral fibers in the CA1.

To determine the intracellular Ca^{2+} concentration, we measured the fluorescence of fura-2 above 520 nm with a DM510 dichroic mirror and a BA520 emission filter (Nikon, Tokyo, Japan). The excitation wavelength was cycled between 340 nm and 380 nm with a rotary excitation wheel. For the NMDA-induced Ca^{2+} measurements, the time sequence was as follows: 340-nm exposure for 1 s; 380-nm exposure for 1 s; closure for 3 s; 340-nm exposure for 1 s; 380-nm exposure for 1 s; etc. The time resolution of measurement was thus 5 s. For the tetanus-induced Ca^{2+} measurements, the time sequence was as follows: 340-nm exposure for 0.75 s; 380-nm exposure for 0.75 s; closure for 0.5 s; 340-nm exposure for 0.75 s; 380-nm exposure for 0.75 s; etc. The time resolution of measurement was thus 2 s. The intracellular Ca^{2+} concentration is expressed as f_{340}/f_{380} , the ratio of fura-2 fluorescence intensity at 340-nm excitation (f_{340}) to that at 380 nm excitation (f_{380}).

Procedure for Measurement of Long-Term Potentiation

The setup was the same as NO imaging, and a monopolar tungsten-stimulating electrode was placed along the Schaffer collateral fibers in the CA1, inducing a response that was 50% of the maximum field excitatory postsynaptic potential (fEPSP) at 0.05 Hz. fEPSP was recorded from stratum radiatum of CA1 with a glass microelectrode filled with ACSF. The distance between electrodes was $\sim 150 \mu\text{m}$, corresponding roughly to a rectangle "sr3" in Figure 4A. For tetanic stimulation (20 V) (SanMartin et al., 1999), a single pulsed stimulus at 100 Hz was delivered for 1 s (stimulus duration, 100 μ s).

Statistical Analysis

All data are expressed as mean \pm SD, except where otherwise noted. The Student's t -test (for two groups) and ANOVA, followed by the Tukey multiple comparison test (for three or more groups) were used to determine the statistical significance of differences.

RESULTS

Spatiotemporal Patterns of NO Production upon NMDA Stimulation

The fluorescence intensity of the DAR-loaded hippocampal slices was measured to determine NO production. Fluorescence

intensities in the CA1, CA3, and DG were examined using a set of square regions, numbered 1–12 (Fig. 1A). Upon 1 mM NMDA stimulation, a transient increase in DAR fluorescence intensity, assessed as the average of squares 1–12 in the CA1, CA3, or DG, was observed. Figure 1B shows the time course of DAR fluorescence in the CA1. Because the reaction of NO with DAR is irreversible, DAR fluorescence intensity remains stable after reaction with NO. The DAR fluorescence intensity is therefore indicative of the cumulative NO production at the time of measurement. To assess the transient NO production at each time, t , consecutive pairs of DAR fluorescence intensity measurements were subtracted to obtain $\Delta f(t) = f(t+5 \text{ s}) - f(t \text{ s})$ (Fig. 1C); see Materials and Methods). Hereafter, $\Delta f(t)$ is used to denote DAR fluorescence increase at time, t . The initial fluorescence intensity (i.e., before NMDA stimulation) was assigned as the autofluorescence of the hippocampal slices, since this fluorescence was not reduced by treatment of L-NMMA (a NOS inhibitor; data not shown).

The time course of the DAR fluorescence increase, $\Delta f(t)$ in the CA1 attendant upon 1 mM NMDA stimulation is illustrated in Figure 1C. A similar time course was observed in the CA3 and DG. DAR fluorescence increase was greatest immediately after stimulation. The maximal value of $\Delta f(t)$ was 2.86 ± 0.73 (CA1), 0.95 ± 0.48 (CA3) and 0.89 ± 0.53 (DG), respectively (6 slices each). The peak measurement in the CA1 was significantly greater than that in the CA3 or DG. After reaching a maximum value, DAR fluorescence increase gradually decreased in a time-dependent fashion, and ceased within 1.5 min. A comparison of the gross amount of DAR fluorescence increase upon NMDA stimulation, among the CA1, CA3, and DG region was undertaken by integrating the DAR fluorescence increase, $\Delta f(t)$ observed in each region, over the 1.5-min time interval immediately after the stimulation (see Fig. 1C,E). The total amount of DAR fluorescence increase in the CA1 (13.7 ± 2.4) exceeded that in either the CA3 (6.6 ± 0.7) or DG (7.7 ± 2.1) (Fig. 1E). The time course of the DAR fluorescence increase measured in subregions of the CA1 is illustrated in Figure 2A. The total amount of DAR fluorescence increase in each subregion was calculated as previously described (Fig. 2B). In the CA1, the gross amount of DAR fluorescence increase measured in the stratum radiatum (sr; 18.0 ± 3.1) was significantly greater than that in either the stratum oriens (so) (12.1 ± 3.2) or the pyramidal cell layer (pcl) (10.8 ± 1.7) (Fig. 2B). In the CA3 and DG, no significant variation was observed among the gross amounts of NO produced in the various subregions (In the CA3: so, 5.3 ± 1.7 ; pcl, 6.8 ± 1.9 ; sr, 7.4 ± 2.4 . In the DG: molecular layer (ml), 9.6 ± 5.2 ; granular layer (gl), 6.4 ± 1.1 ; polymorphic layer (pl), 7.2 ± 2.1). Figure 2C illustrates representative two-dimensional images of the DAR fluorescence increase measured in the CA1, CA3, and DG. Treatment with 300 μM L-NMMA from 20 min before NMDA stimulation significantly inhibited DAR fluorescence increase (Fig. 1D,E), demonstrating that the fluorescence increase of DAR-4M upon the stimulation reflects NO production, and that this NO was due to NOS.

NMDA-Induced Ca^{2+} Response in the CA1, CA3, and DG

The Ca^{2+} response was measured to examine whether the amount of NO produced in the various hippocampal subregions is

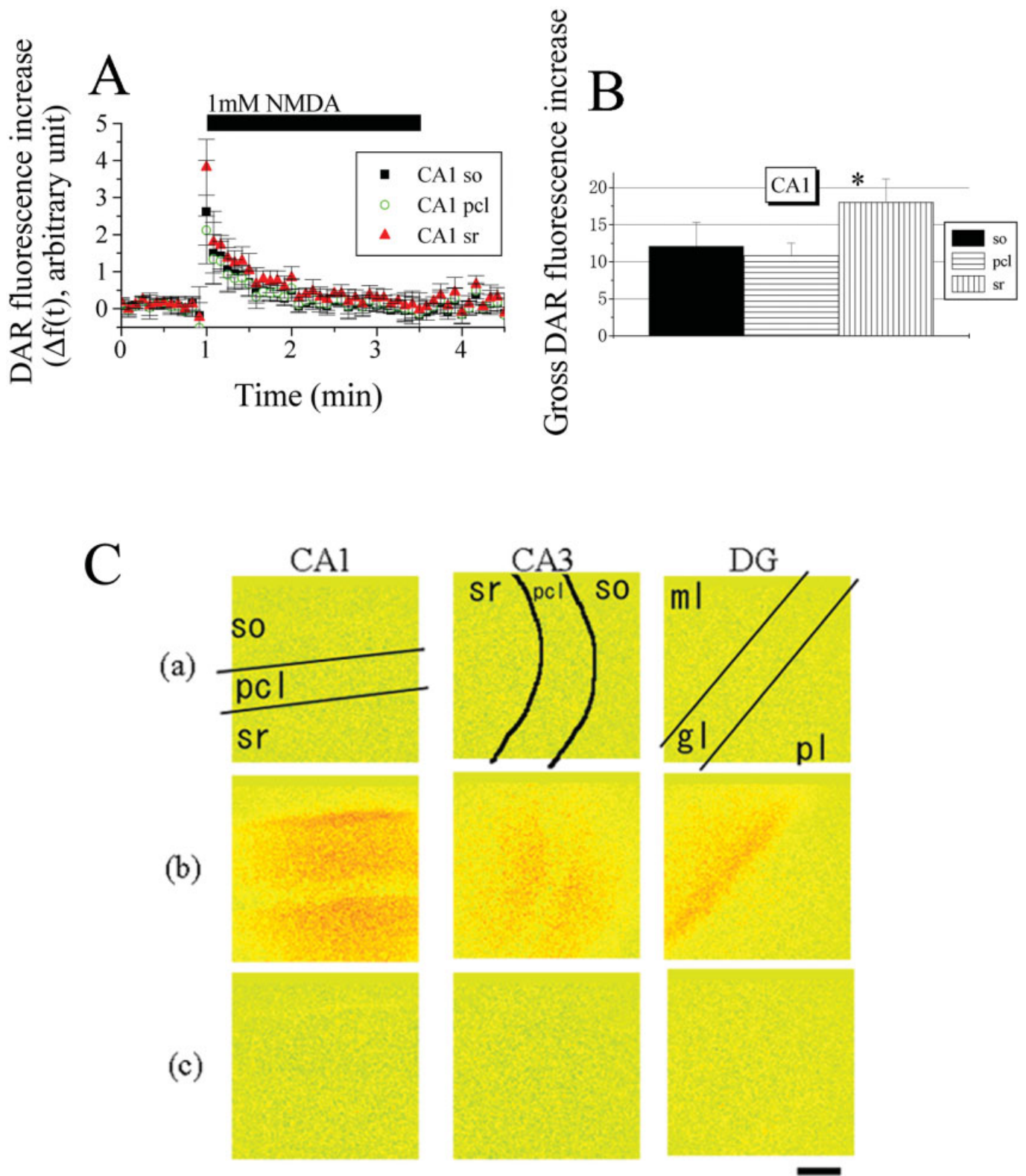


FIGURE 2. NMDA-induced DAR fluorescence increase in subregions of the CA1. **A:** Time course of DAR fluorescence increase [$\Delta f(t)$] obtained by subtracting consecutive pairs of DAR-4M fluorescence intensity [$f(t)$], over squares 1–4 (so), 5–8 (pcl), or 9–12 (sr). Closed bar above the graph designates the period of NMDA perfusion. **B:** Comparison of the gross amount of DAR fluorescence increase in subregions of the CA1. The gross amount was obtained by summing the DAR fluorescence increase [$\Delta f(t)$] from the beginning of NMDA stimulation to 1.5 min after the stimulation. * $P < 0.05$. Data depict averages (\pm SD) from six slices. **C:** Representative two-

dimensional images of DAR fluorescence increase in the CA1, CA3, and DG upon NMDA stimulation: (a) 1 min before NMDA stimulation; (b) 5 s after stimulation; (c) 2 min after stimulation. Images were obtained by subtracting consecutive DAR-4M-fluorescence images, i.e., $\Delta f(t) = f(t + 5 \text{ s}) - f(t \text{ s})$; $t = 0 \text{ s}$ for (a), $t = 60 \text{ s}$ for (b), $t = 180 \text{ s}$ for (c). Lines indicate the pcl in the CA1 and CA3, and the gl in the DG. DAR fluorescence increase is pseudo-color-coded green (low) to red (high). Scale bar = 100 μm . [Color figure can be viewed in the online issue, which is available at www.interscience.wiley.com.]

proportional to the magnitude of the associated Ca^{2+} response. As in the NMDA-induced NO experiments, the fluorescence ratio of fura-2 (f340/f380) in the CA1, CA3, and DG was examined using a set of square regions, numbered 1–12. In comparison with a brightfield image, squares 1–4, 5–8, 9–12 were placed at the so, pcl, and sr, respectively in the CA1 and CA3. In the DG, squares 1–4, 5–8, 9–12 were placed at the ml, gl, and pl, respectively. After 1 mM NMDA stimulation, a transient increase in the fura-2 ratio, assessed as the average of squares 1–12 in the CA1, CA3, or DG, was observed (Fig. 3A). The calcium response (f340/f380) was maximal just after the stimulation. The peak ratio was 0.89 ± 0.04 in CA1 (8 slices), 0.81 ± 0.04 in CA3 (6 slices), and 0.90 ± 0.07 in DG (7 slices) (Fig. 3B). The peak values in the CA1 and DG were nearly identical, and significantly greater than that in the CA3. After reaching a peak value, the fura-2 ratio declined to a constant, but still elevated level (0.72 ± 0.06 in CA1, 0.70 ± 0.05 in CA3, and 0.75 ± 0.08 in DG). The time course of the Ca^{2+} response in the so, pcl, and sr of the CA1 is shown in Figure 3C. Figure 3D compares the peak values of the Ca^{2+} response in subregions among the CA1, CA3, and DG. In the CA1, the peak value in the pcl (0.92 ± 0.07) was significantly greater than that in the so (0.84 ± 0.10). In the CA3, the peak value in the pcl (0.86 ± 0.05) was significantly greater than that in the so (0.77 ± 0.05). In the DG, the peak value in the gl (0.97 ± 0.08) was significantly greater than that in the ml (0.89 ± 0.09), and that in the pl (0.84 ± 0.05). Figure 3E illustrates representative two-dimensional images of the Ca^{2+} response in the CA1, CA3, and DG.

Spatiotemporal Patterns of Tetanus-Induced NO Production in the CA1

Since NO is known to be involved in LTP in the CA1, we next examined the NO production attendant upon tetanic stimulation in the region. The experimental arrangement for tetanic stimulation is illustrated in Figure 4A; an electrode was placed at a rectangle, “sr1” of the CA1. The fluorescence intensity of the DAR-loaded hippocampal slices was examined in a set of rectangular regions. Four rectangular boxes were placed in the so, pcl, and sr subregions, as shown in the brightfield image. To cover each hippocampal region and to improve the signal-to-noise ratio, boxes in the sr are larger than boxes in the so and pcl. Average DAR fluorescence increase in each square was analyzed.

After tetanic stimulation with 20 V, the DAR fluorescence increase was observed in all rectangular subregions in the CA1. Figure 4B1 illustrates the DAR fluorescence increase in the sr of the CA1. The DAR fluorescence increase in the so, pcl, and sr, expressed in terms of $\Delta f(t)$, was greatest immediately after the stimulus. The maximum value observed in each of the CA1 subregions is shown in Table 1a. The maximum value $\Delta f(t = 1.6 \text{ min})$ observed in the sr1 was significantly greater than that in either the so1 or pcl1. Similarly, maximum values in the sr2 and sr3 were significantly greater than that in the “so2 or pcl2” or “so3 or pcl3,” respectively. After reaching a maximal value, DAR fluorescence increase decreased gradually, and ceased within approximately 1.5 min. When this study was repeated, using one-half of the stimulation intensity (10 V), similar results were obtained with decreased

peak DAR fluorescence increase, as shown in Table 1a. Comparison of the total amount of DAR fluorescence increase upon tetanic stimulation (20 V) was performed by summing over the DAR fluorescence increase, $\Delta f(t)$, observed from 1.6 min to 3.1 min after the stimulus, as shown in Figure 4B1,C and Table 1b. In the sr, the gross DAR fluorescence increase was largest at the vicinity of a stimulating electrode and decreased with increasing distance from the stimulating electrode, i.e., $82.7 \text{ (sr1)} > 72.3 \text{ (sr2)} > 53.5 \text{ (sr3)} > 37.3 \text{ (sr4)}$. In the so and pcl, no significant variation was observed in the gross DAR fluorescence increase among the pcl1–4, and the so1–4, respectively. The gross DAR fluorescence increase in the sr1 was greater than that in the pcl1 or so1. Similarly, DAR fluorescence increase in the sr2 and sr3 was significantly greater than that in “so2 or pcl2” or “so3 or pcl3,” respectively. When one-half of the stimulation intensity (10 V) was used, similar results were obtained with a smaller gross DAR fluorescence increase, as shown in Table 1b. Figure 4E illustrates representative two-dimensional images of the DAR fluorescence increase, at 1 min before, immediately after, and 1 min after tetanic stimulation (20 V), respectively. Treatment with an NOS inhibitor (300 μM L-NMMA) from 20 min before stimulation significantly inhibited DAR fluorescence increase (Fig. 4D). In Figure 4B2, LTP induced upon a tetanic stimulation (20 V) is shown. A recording electrode was placed 150 μm from a stimulation electrode, corresponding to “sr3” in Figure 4A.

Tetanic Stimulation-Induced Ca^{2+} Response in the CA1

To investigate whether the amount of DAR fluorescent increase observed among the CA1-subregions is dependent on the magnitude of the Ca^{2+} response, the ratio of the fluorescence intensities (f340/f380) in the CA1 of fura-2-loaded hippocampal slices was examined using a set of rectangular regions. As in the tetanus-induced NO experiment, four rectangles were placed in the so, pcl, and sr, respectively, by comparison with a brightfield image. In the same manner as described for the NO experiments, an electrode, used to deliver tetanic stimulation, was placed at a rectangle “sr1.”

Upon stimulation, a transient Ca^{2+} response (f340/f380) was observed in all subregions of the CA1. Figure 5A illustrates the

FIGURE 3. NMDA-induced Ca^{2+} response in the hippocampus. **A:** Time course of fura-2 ratio, averaged over squares 1–12 in the CA1, CA3, and DG. Closed bar above the graph designates the period of NMDA stimulation. Data are averages (\pm SD) from six to eight slices. **B:** Comparison of the peak amplitude of fura-2 ratio after the stimulation. $*P < 0.05$. Data depict averages (\pm SD) from six to eight slices. **C:** Time course of fura-2 ratio in subregions of the CA1 upon NMDA stimulation. Averages over squares 1–4 (so), 5–8 (pcl), and 9–12 (sr) in the CA1 are shown. **D:** Comparison of the peak amplitude of the fura-2 ratio in subregions of the CA1, CA3, and DG after the stimulation. $*P < 0.05$. Data are averages (\pm SD) from six to eight slices. **E:** Representative two-dimensional images of the Ca^{2+} response (fura-2 ratio) in the CA1, CA3, and DG upon NMDA stimulation: (a) 1 min before the stimulation; (b) 5 s after the stimulation; (c) 2 min after the stimulation. Lines indicate the pcl in the CA1 and CA3, and the gl in the DG. Ca^{2+} response is pseudo-color-coded blue (low) to white (high). Scale bar = 100 μm . [Color figure can be viewed in the online issue, which is available at www.interscience.wiley.com.]

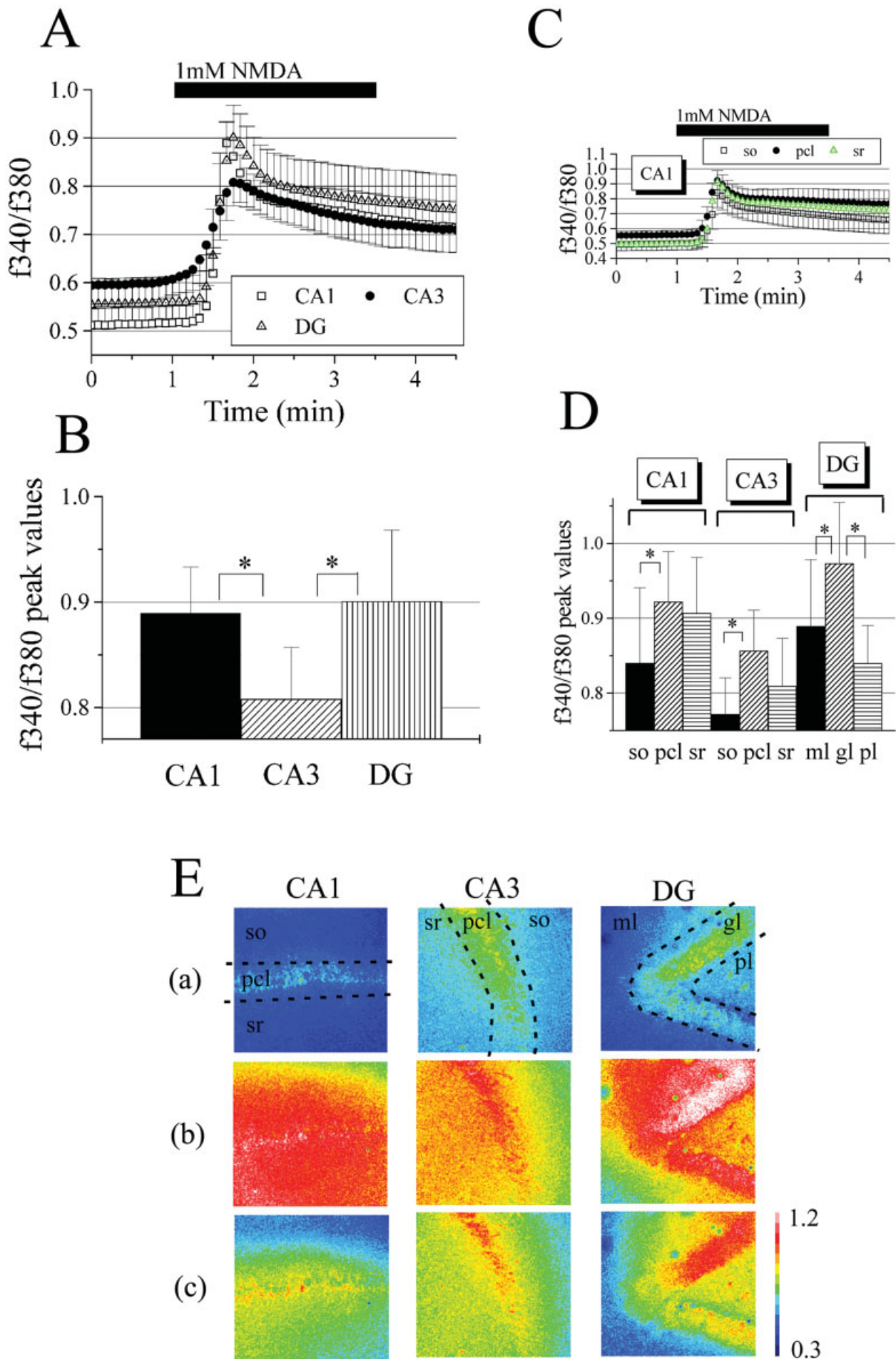


FIGURE 3

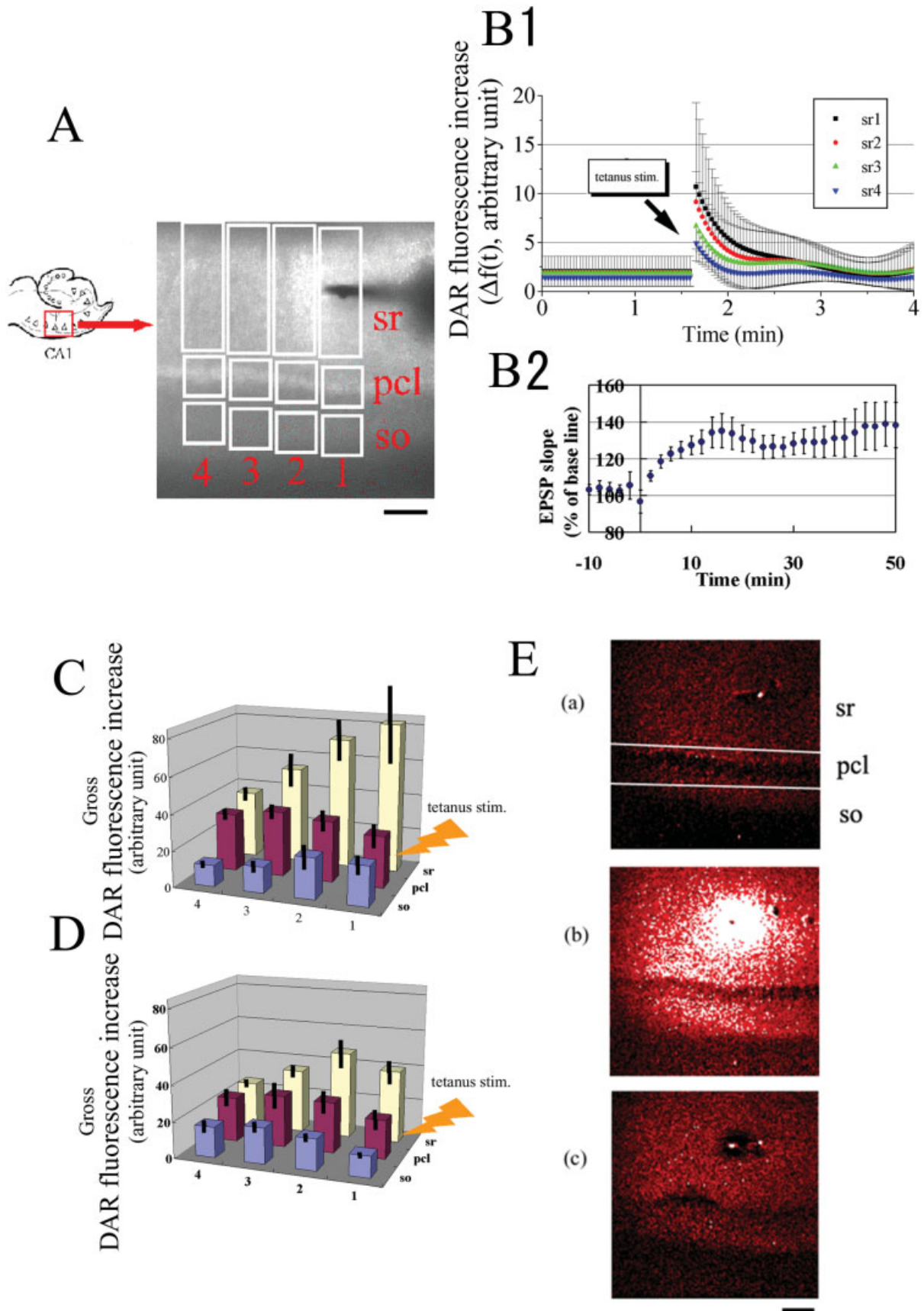


FIGURE 4

time course of this response in the sr. The Ca^{2+} response was greatest just after the stimulation. After reaching a peak value, the intracellular Ca^{2+} concentration decreased gradually. Figure 5B and Table 2 indicate the maximum value of the Ca^{2+} response in each square upon a tetanic stimulation (20 V). In the sr, Ca^{2+} response was largest at the vicinity of a stimulating electrode and decreased as a function of increasing distance from the electrode, i.e., 0.35 (sr1) $>$ 0.34 (sr2) $>$ 0.31 (sr3) $>$ 0.29 (sr4). The Ca^{2+} responses in the sr1 and pcl1 were significantly larger than that in the so1. Similarly, that in "sr2 and pcl 2" and "sr3 and pcl 3" was significantly larger than that in so2 or so3, respectively. When the stimulation intensity was decreased to one-half (10 V), similar results were obtained with decreased peak Ca^{2+} response (Table 2). Figure 5C illustrates a representative two-dimensional image of the Ca^{2+} response, at 1 min before, immediately after, and 1 min after the tetanic stimulation (20 V), respectively.

DISCUSSION

Heterogeneous NO production was demonstrated using real-time two-dimensional NO imaging in hippocampal slices upon NMDA and tetanic stimulation. The results are essential to understand variations in the physiological effects of NO between the CA1, CA3 and DG regions, and in the so, pcl, and sr subregions.

Advantage of NO-Reactive DAR Dye

Digital fluorescence imaging using an NO-reactive fluorescent dye has the strong advantage of allowing the investigation of two-dimensional NO production in real-time, which is impossible with conventional procedures employing NO electrodes, citrulline assay, or electron spin resonance analysis (Kojima et al., 1998b, 1999). NO imaging in the hippocampus, after NMDA stimulation was first reported by Kojima et al., employing the NO-reactive fluorescent dye, DAF-2 (Kojima et al., 1998a). However, the NO production in hippocampal neurons has been difficult to detect reproductively via DAF-2, due to: (1) the pH dependence of DAF-2, whose fluorescence intensity decreases sharply below pH 7.0 (Kojima et al., 1998b); and (2) the decrease in the intracellular

pH of hippocampal neurons in the CA1 from 7.2 to approximately 6.0 upon NMDA stimulation (Yamamoto et al., 1998; Zhan et al., 1998). We subsequently reported NO imaging in the CA1 upon 1 mM NMDA stimulation, in which DAF-FM (an improved DAF-2 type dye, whose fluorescence intensity is pH-independent above pH 5) was used in order to avoid the DAF-fluorescence decrease typical upon acidification of neuronal pH by NMDA stimulation (Takata et al., 2002). The use of a modified ACSF, however was necessary to completely avoid the fluorescence decrease. Although we employed DAF-FM, we were unable to observe a difference in the NO production among the so, pcl, and sr in the CA1, due to the low signal-to-noise ratio of DAF-FM. In addition, we were unable to compare the NO production between the CA1, CA3, and DG using DAF-FM, due to a weak fluorescence increase upon NO production in the CA3 and DG, which was below the background fluorescence (unpublished data). In the present study, DAR-4M was employed. DAR-4M is an improved DAF-2 type dye, which employs a rhodamine rather than fluorescein fluorophore. The use of DAR-4M enabled us to measure such a weak NO production in conventional ACSF, because DAR fluorescence intensity is pH-independent above 4.0 (Kojima et al., 2001). Moreover, a longer excitation wavelength of 520–540 nm of DAR-4M resulted in smaller background fluorescence of hippocampal slices than those observed with DAF-2 or DAF-FM, resulting in an improved signal-to-noise ratio in the imaging. Although both divalent cation (Ca^{2+} and Mg^{2+}) sensitivity and the photoactivation of DAF-2 had been suggested in the report using NO donors (Broillet et al., 2001), the observed sensitivities has been shown to be derived from the interaction of either the metal cation or intense light with the NO donors, and therefore the reaction of DAF-2 and NO should be independent of Ca^{2+} , Mg^{2+} , and light (Suzuki et al., 2002). Because DAF-2 fluorescence has been shown to be quenched by the presence of micromolar concentrations of either dehydroascorbic acid or ascorbic acid (Zhang et al., 2002), which could be present in the brain, the currently observed fluorescence increase of DAR-4M might be larger in the absence of these substances in the hippocampus.

FIGURE 4. Tetanus-induced DAR fluorescence increase in the CA1. **A:** Region used for imaging of tetanus-induced NO. Left: Illustration of a hippocampal slice. Red square indicates the region for imaging. Right: Representative brightfield image of the CA1 of a DAR-4M-loaded hippocampal slice. Vague shadow at the upper right is an electrode for tetanic stimulation. Squares were placed at the so, pcl, and sr, numbered from 1 (nearest to an electrode) to 4 (most distant from an electrode). Average DAR fluorescence increase in each square was analyzed. Scale bar = 100 μm . **(B1)** Time course of DAR fluorescence increase in the sr of the CA1 upon tetanic stimulation, as indicated by an arrow in the graph ($t = 1.6$ min). Data depict averages (\pm SD) from eight slices. **(B2)** LTP induction was shown as the time course of fEPSP response measured with a recording electrode separated from a stimulating electrode ~ 150 μm , corresponding to "sr3" in A. Tetanic stimulation was delivered at time = 0. Data are averages (\pm SEM) from 4 slices. **C:** Comparison of the gross DAR fluorescence increase upon tetanic stimulation. The gross amount was obtained by

summing the DAR fluorescence increase [$\Delta f(t)$] from at the time of tetanic stimulation to 1.5 min after the stimulation. Data are averages (\pm SEM) from eight slices. **D:** Gross DAR fluorescence increase in the presence of a NOS inhibitor. Hippocampal slices were perfused with ACSF containing 300 μM L-NMMA from 20 min before the stimulation to the end of the measurement. Data depict averages (\pm SEM) from eight slices. **E:** Representative two-dimensional images of gross DAR fluorescence increase in the CA1 upon tetanic stimulation. (a) 1 min before tetanic stimulation; (b) 5 s after the stimulation; (c) 1 min after the stimulation. Gross DAR fluorescence increase was performed by summing the DAR fluorescence increase [$\Delta f(t)$] from 0.6 min to 1.6 min, 1.6 min to 3.2 min, 3.2 min to 4.8 min for (a–c), respectively (see Fig. 4B1). Tetanic stimulation was delivered at 1.6 min. White lines indicate the pcl. DAR fluorescence increase is pseudo-colored black (lowest), red (middle), and white (highest). Scale bar = 100 μm . [Color figure can be viewed in the online issue, which is available at www.interscience.wiley.com.]

TABLE 1.

Fluorescence Increase upon Tetanic Stimulation*

| | 1 | 2 | 3 | 4 |
|-----|------------------------------|------------------------------|----------------------------|----------------------------|
| | | (a) Maximal DAR ^a | | |
| sr | 10.7 ± 8.6 (2.5 ± 1.9) | 9.2 ± 3.1 (3.0 ± 2.1) | 6.7 ± 2.3 (2.7 ± 1.7) | 4.9 ± 1.8 (1.6 ± 1.1) |
| pcl | 3.0 ± 2.1 (1.8 ± 1.9) | 3.7 ± 1.7 (2.0 ± 1.9) | 4.2 ± 1.5 (1.9 ± 1.4) | 3.8 ± 1.8 (1.2 ± 0.9) |
| so | 2.5 ± 1.4 (1.5 ± 1.6) | 2.5 ± 1.7 (1.8 ± 1.6) | 2.0 ± 0.8 (1.5 ± 1.4) | 1.7 ± 1.0 (0.9 ± 0.7) |
| | | (b) Gross DAR ^b | | |
| sr | 82.7 ± 21.5 (24.9 ± 10.4) | 72.3 ± 10.8 (29.6 ± 11.1) | 53.5 ± 7.5 (27.7 ± 6.1) | 37.3 ± 4.2 (18.2 ± 4.0) |
| pcl | 28.4 ± 7.2 (18.8 ± 8.8) | 33.6 ± 6.7 (20.1 ± 7.3) | 36.1 ± 5.5 (18.5 ± 3.6) | 31.9 ± 4.4 (13.0 ± 2.1) |
| so | 21.7 ± 5.4 (13.6 ± 9.5) | 22.7 ± 7.1 (15.3 ± 10.1) | 14.3 ± 3.1 (12.5 ± 6.5) | 11.8 ± 2.0 (7.3 ± 1.8) |

*Numbers in parentheses represent data resulting from 10 V tetanic stimulation.

^aMaximal values of DAR fluorescence increase, Δf at 1.6 min, upon tetanic stimulation (20 or 10 V) are shown (mean ± SD from 8 slices). Numbers 1–4 indicate the position of NO imaging, as illustrated in Fig. 4A. 1 is nearest to a stimulating electrode, and 4 is most distant from the electrode in each area of so, pcl, or sr.

^bGross amount of DAR fluorescence increase, obtained by summing the DAR fluorescence increase [$\Delta f(t)$] from at the time of tetanic stimulation (1.6 min) to 1.5 min after the stimulation (20 or 10 V), is shown (mean ± SEM from 8 slices). Positioning numbers of NO imaging from 1 to 4 are the same as (a).

Heterogeneous NO Production upon NMDA Stimulation

The observed net DAR fluorescence increase was heterogeneous among the CA1, CA3, and DG regions. Net DAR fluorescence increase in the CA1 upon NMDA stimulation was approximately twice that observed in the CA3 and DG (Fig. 1E), suggesting greater productivity of NO in CA1. This result may be related to the observation that the CA1 is much more vulnerable to NMDA-induced neurotoxicity than the CA3 and DG, even though the measured Ca^{2+} influx in the CA1 and DG was approximately identical (but see Keynes et al., 2004; Kiyota et al., 1991; Kudo et al., 1991). The DAR fluorescence increase was also observed to vary among the subregions of the CA1. The DAR fluorescence increase in the sr was approximately 1.5 times greater than that in the so and pcl (Fig. 2B), suggesting heterogeneous NO production among these regions. These results may be related to the observation that NO is necessary for the induction of LTP in the sr, but not in the so subregion of the CA1 (Haley et al., 1996).

From previous investigations, the localization and enzymatic characters of nNOS have been demonstrated in detail. For example, (1) principal neurons in the hippocampus contain nNOS (Endoh et al., 1994; Iwase et al., 1998; Takata et al., 2002); (2) nNOS is associated with NMDA receptors by PSD-95 at postsynapses, as demonstrated by immunoelectron microscopy and immunoprecipitation (Christopherson et al., 1999; Valtschanoff and Weinberg, 2001); and (3) nNOS is a calcium-dependent enzyme (An-

drew and Mayer, 1999). The net DAR fluorescence increase observed in several regions was not always proportional to the magnitude of Ca^{2+} response upon NMDA stimulation. Although the magnitudes of the Ca^{2+} response in the CA1 and DG were nearly equal, the amount of DAR fluorescence increase in the CA1 was twice that produced in the DG (Figs. 1E and 3B). In the CA3, however, both the magnitude of the Ca^{2+} response and the net DAR fluorescence increase corresponded to the smallest values observed in the hippocampus. It should be noted that the ratio of fura-2 fluorescence (f340/f380) was not saturated in the current experimental condition as described in our previous investigation (Takata et al., 2002). Moreover, we confirmed that fura-2 ratio did not saturate at least up to 2.0, where $[\text{Ca}^{2+}]_i$ was 900 nM, using Ca^{2+} ionophore added to Chinese hamster ovary (CHO) cells loaded with fura-2 (data not shown). Therefore, the observed nearly identical Ca^{2+} responses in CA1 and DG should not be an artifact. One possible explanation for the nonproportional relation between Ca^{2+} response and DAR fluorescence increase is that nNOS expression in the CA1 may be larger than that in the DG. The heterogeneous level of expression for PSD-95 and CAPON (an inhibitor protein of nNOS) may also induce a nonproportional response relationship between the NO production and the accompanying Ca^{2+} increase (Christopherson et al., 1999; Endoh et al., 1994; Jaffrey et al., 1998). Other possibility is that the Ca^{2+} response measured with fura-2 may not be a good indicator of Ca^{2+} concentration at the position of nNOS located in the vicinity of NMDA receptors (Valtschanoff and Weinberg, 2001).

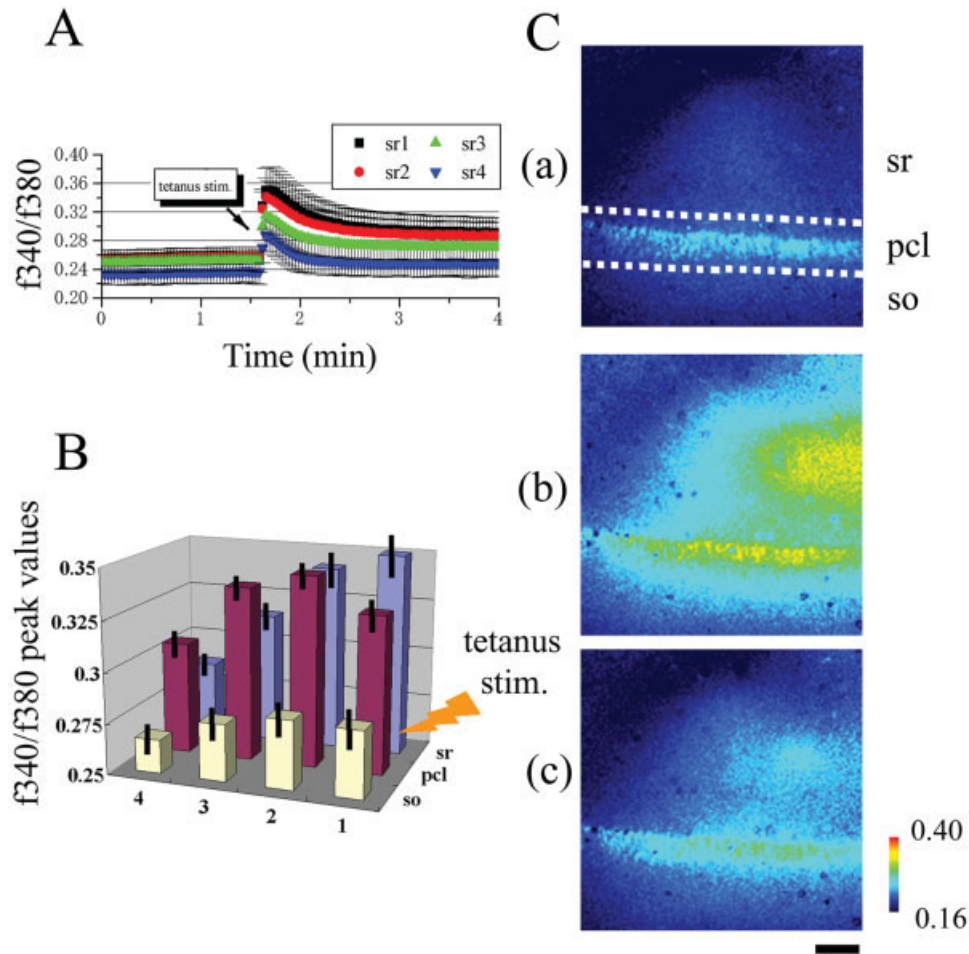


FIGURE 5. Tetanus-induced Ca^{2+} response in the CA1. **A:** Time course of the Ca^{2+} response in the sr of the CA1 upon stimulation indicated by an arrow in the graph. Data depict averages (\pm SD) from eight slices. **B:** Comparison of the peak values of fura-2 ratio in the CA1 after stimulation. Data are averages (\pm SEM) from eight slices. **C:** Representative two-dimensional images of the Ca^{2+} response (fura-2 ratio, f_{340}/f_{380}) in the CA1 upon tetanic stimulation. (a) 1 min

before tetanic stimulation; (b) 5 s after stimulation; (c) 1 min after stimulation. Electrode for tetanic stimulation was placed at square "sr1" as in the NO experiments (see Fig. 4A). Ca^{2+} response is pseudo-color-coded blue (low) to white (high). White lines indicate the pyramidal cell layer. Scale bar = 100 μm . [Color figure can be viewed in the online issue, which is available at www.interscience.wiley.com.]

In addition to nNOS, eNOS may exist in the hippocampus (Dinerman et al., 1994). The relative contributions of nNOS and eNOS to the NO production were not clarified in the present study. NOS activity in homogenates of hippocampal tissue from nNOS knockout mice measured by citrulline assay was only 1.7–3.9% of that obtained from wild mice (Huang et al., 1993; Son et al., 1996). These results imply that the contribution of eNOS to total NO production is very small in the hippocampus. The DAR fluorescence increase in our study may therefore be mainly due to nNOS.

It was previously reported that the extracellular concentration of NO reaches 2.2 ± 0.1 nM after electrical stimulation (10 Hz, 2 s) of a cerebellar slice, using an NO electrode (Kimura et al., 1998). Due to the difficulty of measurement, however few reports have been published regarding NO concentration in the hippocampus. In this study, we have attempted to estimate the concentration of NO in the CA1 after NMDA stimulation. The rate of DAR-fluorescence increase upon reaction with NO was estimated

TABLE 2.

*Maximal Ca^{2+} Response upon Tetanic Stimulation**

| | 1 | 2 | 3 | 4 |
|-----|--|--|--|--|
| sr | 0.35 ± 0.01 (0.30 ± 0.01) | 0.34 ± 0.01 (0.31 ± 0.02) | 0.31 ± 0.01 (0.29 ± 0.02) | 0.29 ± 0.01 (0.27 ± 0.02) |
| pcl | 0.33 ± 0.01 (0.31 ± 0.02) | 0.34 ± 0.01 (0.32 ± 0.01) | 0.34 ± 0.01 (0.31 ± 0.01) | 0.31 ± 0.01 (0.29 ± 0.01) |
| so | 0.28 ± 0.01 (0.27 ± 0.02) | 0.28 ± 0.01 (0.27 ± 0.03) | 0.28 ± 0.01 (0.26 ± 0.03) | 0.27 ± 0.01 (0.25 ± 0.02) |

*Maximal values of Ca^{2+} response, f_{340}/f_{380} at 1.6 min, upon tetanic stimulation (20 or 10 V) are shown (mean \pm SEM from 8 slices). Numbers in parentheses represent data from 10 V tetanic stimulation. Positioning numbers of NO imaging from 1 to 4 are the same as Table 1(a).

using the molar absorption coefficient (ϵ [$M^{-1} \cdot cm^{-1}$]; DAR-4M, 7.8×10^4 ; DAR-4M T, 7.6×10^4), quantum yield (Φ ; DAR-4M, 0.0005; DAR-4M T, 0.42), the equation for the steady state fluorescence intensity ($F = 2.303 \cdot I_e C \cdot \Phi$, where F is a steady-state fluorescence intensity, I_{ex} is number of photons per time per unit area, C is the molarity of a fluorescence dye in ground state), and the assumptions that (1) the reaction rate of DAR-4M with NO is $\sim 20\%$ (note that this rate was obtained using a cell-free assay, and the reaction rate within cells could be lower, which may result in an underestimation of NO concentration) (Kinosita and Mihashi, 1983; Kojima et al., 2001); (2) 10 μM DAR-4M is distributed uniformly throughout hippocampal slices; and (3) the background fluorescence of slices is negligible. Calculations indicate that DAR fluorescence intensity increases by 42.9% when a solution of 10 μM DAR-4M reacts with 20 nM NO. Because 1 mM NMDA stimulation induced an 8.9% increase ($=2.86/32$; see Fig. 1B) in DAR-fluorescence in the CA1, the concentration of intracellular NO upon NMDA stimulation was estimated to be 4.2 nM, which was in good accordance with other reports (Keynes et al., 2004).

Tetanic Stimulation-Induced NO Production in the CA1

The present results demonstrated that NO production upon tetanic stimulation was largest at the vicinity of a stimulating electrode and decreased as a function of increasing distance from the stimulating electrode. These results suggest the possibility that the effect of NO in LTP is dependent on differences in NO concentration caused by the distant dependent NO production from a stimulating electrode. This concentration difference, dependent on distance between a stimulating and a recording electrode, may be a key factor to resolve previous controversial results about positive and negative effects of NO in LTP (Hawkins et al., 1998). Because studies using NO donors have demonstrated that the physiological effects of NO vary with concentration (Prast and Philippu, 2001), one possible explanation is that the observed differences are due to differences in the concentration of NO produced in the vicinity of the recording electrode in each experiment. Low concentrations of SNAP (an NO donor) decreased glutamate release in the hippocampus, thereby inhibiting LTP induction. On the other hand, the use of high SNAP concentrations enhanced glutamate release (Segieth et al., 1995), thereby enhancing LTP induction. As to effects of NO on LTP, three cases are reported: (A) NOS inhibitors blocked the induction of LTP in the CA1 (Bohme et al., 1991; Doyle et al., 1996; Haley et al., 1992; O'Dell et al., 1991; Schuman and Madison, 1991), (B) NOS inhibitors failed to block LTP induction (Bannerman et al., 1994), and (C) NOS inhibitors facilitated LTP induction (Kato and Zorumski, 1993). These contradictory observations might be due to the difference in NO production, i.e., case (A) has high NO production (facilitating LTP), case (B) has medium NO production (having no effect on LTP), and case (C) has low NO production (inhibiting LTP). In previous reports on the effect of NO on LTP in the CA1, the distance between a stimulating

electrode and a recording electrode was arbitrarily set at an unspecified distance, which probably ranged from 100 to 500 μm . Consequently, it would be necessary to know NO concentration in previous reports in order to explain their observation of positive or negative contribution of NO to LTP induction. Therefore, the current observation of NO concentration is of great importance. It should be noted, however, that our observation of the distant dependent NO production may include an artifact, because during preparation of slices by a tissue slicer, some of endogenous neuronal circuits were cut. As a result, in a slice preparation, the propagation of the stimulation impulse would be limited to the vicinity of the stimulation electrode. Even so, our observation is applicable to many LTP studies, because slices prepared by a tissue slicer are widely used for LTP investigations. In the present study, we observed LTP without immediate posttetanic potentiation (PTP) for a few minutes just after tetanus (Fig. 4B2). This may be due to a strong tetanic stimulation (20 V), because (1) PTP is generated by an increase of transmitter quanta released by each presynaptic action potential after tetanus, due to residual presynaptic calcium ions (Tang and Zucker, 1997); and (2) a strong stimulation during tetanus may have exhausted readily accessible synaptic vesicles. The similar shape of LTP without PTP has been observed in the cortex (Hensch et al., 1998).

We also found that Ca^{2+} response was not necessarily proportional to NO production upon tetanic stimulation. Although the magnitude of the Ca^{2+} responses in the sr and pcl of the CA1 were not significantly different (Fig. 5B), the amount of DAR fluorescence increase in the sr was 2–3-fold greater than that observed in the pcl (Fig. 4C). Possible explanations for these discrepancies is that (1) a major population of nNOS is localized at synapses where nNOS proteins form a complex with NMDA receptors via PSD-95 proteins (Valtschanoff and Weinberg, 2001; Yun et al., 1996); and (2) the number of synapses in sr may be larger than that in the pcl and so; and (3) nNOS may be driven by the Ca^{2+} beneath the postsynaptic membranes, which is different from cytosolic Ca^{2+} concentration detected with fura-2.

Recently, the spatial distribution of NO production in the hippocampal CA1 region upon theta burst stimulation was measured using the aromatic vicinal diamine, 1,2-diaminoanthraquinone (DAQ) (von Bohlen and Halbach et al., 2002). In their study, NO production was observed mainly in pyramidal cell layer, while our DAR-NO was observed more densely in stratum radiatum than in pyramidal cell layer in the CA1. This discrepancy may depend on the fact that DAR measures only intracellular NO while DAQ is reported to measure both intracellular and extracellular NO. Another significant difference between DAQ and DAR is that DAQ-NO detection was possible only after chemical reaction after the fixation of hippocampal slices. Thus, the time course of NO production in living slices could not be measured in their research.

Acknowledgments

The authors are very grateful to Drs. Hirotatsu Kojima and Tetsuo Nagano at the University of Tokyo for useful advice and discussion on DAR-4M. The authors are also grateful to Mr.

Noboru Fukasaku at Daiichi Pure Chemicals for the synthesis of DAF-FM. This work was supported by a JSPS Research Fellowship for Young Scientists (to N. T.), a Narishige Neuroscience Research Foundation Fellowship (to N. T.), and Special Coordinate Funds for Promoting Science and Technology from the Ministry of Education, Science and Technology, Japan (to S. K.).

REFERENCES

- Andrew PJ, Mayer B. 1999. Enzymatic function of nitric oxide synthases. *Cardiovasc Res* 43:521–531.
- Bannerman DM, Chapman PF, Kelly PA, Butcher SP, Morris RG. 1994. Inhibition of nitric oxide synthase does not prevent the induction of long-term potentiation in vivo. *J Neurosci* 14:7415–7425.
- Bohme GA, Bon C, Stutzmann JM, Doble A, Blanchard JC. 1991. Possible involvement of nitric oxide in long-term potentiation. *Eur J Pharmacol* 199:379–381.
- Bredt DS, Snyder SH. 1990. Isolation of nitric oxide synthetase, a calmodulin-requiring enzyme. *Proc Natl Acad Sci USA* 87:682–685.
- Broillet M, Randin O, Chatton J. 2001. Photoactivation and calcium sensitivity of the fluorescent NO indicator 4,5-diaminofluorescein (DAF-2): implications for cellular NO imaging. *FEBS Letters* 491:227–232.
- Christopherson KS, Hillier BJ, Lim WA, Bredt DS. 1999. PSD-95 assembles a ternary complex with the N-methyl-D-aspartic acid receptor and a bivalent neuronal NO synthase PDZ domain. *J Biol Chem* 274:27467–27473.
- Dinerman JL, Dawson TM, Schell MJ, Snowman A, Snyder SH. 1994. Endothelial nitric oxide synthase localized to hippocampal pyramidal cells: implications for synaptic plasticity. *Proc Natl Acad Sci USA* 91:4214–4218.
- Doyle C, Holscher C, Rowan MJ, Anwyl R. 1996. The selective neuronal NO synthase inhibitor 7-nitro-indazole blocks both long-term potentiation and depotentiation of field EPSPs in rat hippocampal CA1 in vivo. *J Neurosci* 16:418–424.
- Endoh M, Maiese K, Wagner JA. 1994. Expression of the neural form of nitric oxide synthase by CA1 hippocampal neurons and other central nervous system neurons. *Neuroscience* 63:679–689.
- Haley JE, Schaible E, Pavlidis P, Murdock A, Madison DV. 1996. Basal and apical synapses of CA1 pyramidal cells employ different LTP induction mechanisms. *Learn Mem* 3:289–295.
- Haley JE, Wilcox GL, Chapman PF. 1992. The role of nitric oxide in hippocampal long-term potentiation. *Neuron* 8:211–216.
- Hawkins RD, Son H, Arancio O. 1998. Nitric oxide as a retrograde messenger during long-term potentiation in hippocampus. *Prog Brain Res* 118:155–172.
- Hensch TK, Fagiolini M, Mataga N, Stryker MP, Baekkeskov S, Kash SF. 1998. Local GABA circuit control of experience-dependent plasticity in developing visual cortex. *Science* 282:1504–1508.
- Huang PL, Dawson TM, Bredt DS, Snyder SH, Fishman MC. 1993. Targeted disruption of the neuronal nitric oxide synthase gene. *Cell* 75:1273–1286.
- Iwase K, Iyama K, Akagi K, Yano S, Fukunaga K, Miyamoto E, Mori M, Takiguchi M. 1998. Precise distribution of neuronal nitric oxide synthase mRNA in the rat brain revealed by non-radioisotopic in situ hybridization. *Brain Res Mol Brain Res* 53:1–12.
- Jaffrey SR, Snowman AM, Eliasson MJ, Cohen NA, Snyder SH. 1998. CAPON: a protein associated with neuronal nitric oxide synthase that regulates its interactions with PSD95. *Neuron* 20:115–124.
- Kato K, Zorumski CF. 1993. Nitric oxide inhibitors facilitate the induction of hippocampal long-term potentiation by modulating NMDA responses. *J Neurophysiol* 70:1260–1263.
- Keynes RG, Duport S, Garthwaite J. 2004. Hippocampal neurons in organotypic slice culture are highly resistant to damage by endogenous and exogenous nitric oxide. *Eur J Neurosci* 19:1163–1173.
- Kimura S, Uchiyama S, Takahashi HE, Shibuki K. 1998. cAMP-dependent long-term potentiation of nitric oxide release from cerebellar parallel fibers in rats. *J Neurosci* 18:8551–8558.
- Kinosita K, Mihashi K, editors. 1983. *Fluorescence imaging—applications to biological sciences*. Tokyo: Japan Scientific Societies.
- Kiyota Y, Miyamoto M, Nagaoka A. 1991. Relationship between brain damage and memory impairment in rats exposed to transient forebrain ischemia. *Brain Res* 538:295–302.
- Kojima H, Hirofumi M, Nakatsubo N, Kikuchi K, Urano Y, Higuchi T, Hirata Y, Nagano T. 2001. Bioimaging of nitric oxide with fluorescent indicators based on the rhodamine chromophore. *Anal Chem* 73:1967–1973.
- Kojima H, Nakatsubo N, Kikuchi K, Urano Y, Higuchi T, Tanaka J, Kudo Y, Nagano T. 1998a. Direct evidence of NO production in rat hippocampus and cortex using a new fluorescent indicator: DAF-2 DA. *NeuroReport* 9:3345–3348.
- Kojima H, Sakurai K, Kikuchi K, Kawahara S, Kirino Y, Nagoshi H, Hirata Y, Nagano T. 1998b. Development of a fluorescent indicator for nitric oxide based on the fluorescein chromophore. *Chem Pharm Bull* 46:373–375.
- Kojima H, Urano Y, Kikuchi K, Higuchi T, Hirata Y, Nagano T. 1999. Fluorescent Indicators for Imaging Nitric Oxide Production. *Angew Chem Int Ed Engl* 38:3209–3212.
- Kudo Y, Nakamura T, Ito E. 1991. A “macro” image analysis of fura-2 fluorescence to visualize the distribution of functional glutamate receptor subtypes in hippocampal slices. *Neurosci Res* 12:412–420.
- Mizutani A, Saito H, Abe K. 1993. Involvement of nitric oxide in long-term potentiation in the dentate gyrus in vivo. *Brain Res* 605:309–311.
- Nicolarakis PJ, Lin YQ, Bennett MR. 1994. Effect of nitric oxide synthase inhibition on long-term potentiation at associational–commissural and mossy fibre synapses on CA3 pyramidal neurones. *Br J Pharmacol* 111:521–524.
- Nicoll RA, Malenka RC. 1995. Contrasting properties of two forms of long-term potentiation in the hippocampus. *Nature* 377:115–118.
- O’Dell TJ, Hawkins RD, Kandel ER, Arancio O. 1991. Tests of the roles of two diffusible substances in long-term potentiation: evidence for nitric oxide as a possible early retrograde messenger. *Proc Natl Acad Sci USA* 88:11285–11289.
- Prast H, Philippu A. 2001. Nitric oxide as modulator of neuronal function. *Prog Neurobiol* 64:51–68.
- SanMartin S, Gutierrez M, Menendez L, Hidalgo A, Baamonde A. 1999. Effects of diethylstilbestrol on mouse hippocampal evoked potentials in vitro. *Cell Mol Neurobiol* 19:691–703.
- Schuman EM, Madison DV. 1991. A requirement for the intercellular messenger nitric oxide in long-term potentiation. *Science* 254:1503–1506.
- Segieth J, Getting SJ, Biggs CS, Whitton PS. 1995. Nitric oxide regulates excitatory amino acid release in a biphasic manner in freely moving rats. *Neurosci Lett* 200:101–104.
- Son H, Hawkins RD, Martin K, Kiebler M, Huang PL, Fishman MC, Kandel ER. 1996. Long-term potentiation is reduced in mice that are doubly mutant in endothelial and neuronal nitric oxide synthase. *Cell* 87:1015–1023.
- Suzuki N, Kojima H, Urano Y, Kikuchi K, Hirata Y, Nagano T. 2002. Orthogonality of calcium concentration and ability of 4,5-diaminofluorescein to detect NO. *J Biol Chem* 277:47–49.
- Takata N, Shibuya K, Okabe M, Nagano T, Kojima H, Kawato S. 2002. Pregnenolone sulfate acutely enhances NO production in the rat hippocampus: digital fluorescence study using NO reactive dye. *Bioimages* 10:1–8.
- Tang Y, Zucker RS. 1997. Mitochondrial involvement in post-tetanic potentiation of synaptic transmission. *Neuron* 18:483–491.

- Valtschanoff JG, Weinberg RJ. 2001. Laminar organization of the NMDA receptor complex within the postsynaptic density. *J Neurosci* 21:1211–1217.
- von Bohlen, Halbach O, Albrecht D, Heinemann U, Schuchmann S. 2002. Spatial nitric oxide imaging using 1,2-diaminoanthraquinone to investigate the involvement of nitric oxide in long-term potentiation in rat brain slices. *Neuroimage* 15:633–639.
- Wu J, Wang Y, Rowan MJ, Anwyl R. 1997. Evidence for involvement of the neuronal isoform of nitric oxide synthase during induction of long-term potentiation and long-term depression in the rat dentate gyrus in vitro. *Neuroscience* 78:393–398.
- Yamamoto M, Kawanishi T, Kiuchi T, Ohta M, Yokota I, Ohata H, Momose K, Inoue K, Hayakawa T. 1998. Discrepant intracellular pH changes following intracellular Ca^{2+} increases induced by glutamate and Ca^{2+} ionophores in rat hippocampal neurons. *Life Sci* 63:55–63.
- Yun HY, Dawson VL, Dawson TM. 1996. Neurobiology of nitric oxide. *Crit Rev Neurobiol* 10:291–316.
- Zhan RZ, Fujiwara N, Tanaka E, Shimoji K. 1998. Intracellular acidification induced by membrane depolarization in rat hippocampal slices: roles of intracellular Ca^{2+} and glycolysis. *Brain Res* 780:86–94.
- Zhang X, Kim WS, Hatcher N, Potgieter K, Moroz LL, Gillette R, Sweedler JV. 2002. Interfering with nitric oxide measurements. 4,5-diaminofluorescein reacts with dehydroascorbic acid and ascorbic acid. *J Biol Chem* 277:48472–48478.